Neutron Diffraction and Magnetic Susceptibility Studies on a High-Voltage $Li_{1.2}Mn_{0.55}Ni_{0.15}Co_{0.10}O_2$ Lithium Ion Battery Cathode: Insight into the Crystal Structure

ARTICLE *in* CHEMISTRY OF MATERIALS · OCTOBER 2013

Impact Factor: 8.35 · DOI: 10.1021/cm402278q

8 AUTHORS, INCLUDING:

Ashfia Huq
Oak Ridge National Laboratory
116 PUBLICATIONS **1,350** CITATIONS
SEE PROFILE

Edward Andrew Payzant
Oak Ridge National Laboratory
236 PUBLICATIONS **3,518** CITATIONS
SEE PROFILE

Jianlin Li
Oak Ridge National Laboratory
36 PUBLICATIONS **379** CITATIONS
SEE PROFILE

Daniel P. Abraham
Argonne National Laboratory
148 PUBLICATIONS **3,261** CITATIONS
SEE PROFILE

CHEMISTRY OF MATERIALS

Article

pubs.acs.org/cm

Neutron Diffraction and Magnetic Susceptibility Studies on a High-Voltage $Li_{1.2}Mn_{0.55}Ni_{0.15}Co_{0.10}O_2$ Lithium Ion Battery Cathode: Insight into the Crystal Structure

Debasish Mohanty,*[,†] Ashfia Huq,[‡] E. Andrew Payzant,[‡] Athena S. Sefat,[†] Jianlin Li,[§] Daniel P. Abraham,[∥] David L. Wood, III,[§,⊥] and Claus Daniel*[,§,⊥]

[†]Materials Science and Technology Division, [‡]Chemical and Engineering Materials Division, and [§]Energy and Transportation Science Division, Oak Ridge National Laboratory, Oak Ridge, Tennessee 37931, United States

[∥]Chemical Sciences and Engineering Division, Argonne National Laboratory, Argonne, Illinois 60439, United States

[⊥]Bredesen Centre for Interdisciplinary Research and Graduate Education, University of Tennessee, Knoxville, Tennessee 37996, United States

Supporting Information

ABSTRACT: Lithium- and manganese-rich oxides undergo structural transformation and/or atomic rearrangements during the delithiation/lithiation process and ultimately suffer from several issues such as first cycle irreversible capacity and voltage fade. In order to understand the mechanism of these issues, perception of a detailed crystal structure of pristine material is obviously demanding. In this study, combined powder neutron diffraction (ND) and temperature-dependent magnetic susceptibility techniques were employed to investigate the structure of a pristine lithium- and manganese-rich $Li_{1.2}Mn_{0.55}Ni_{0.15}Co_{0.10}O_2$ cathode oxide. Rietveld refinement on the experimental ND pattern yields good fits by considering either Li_2MO_3 (M = Co, Mn, Ni) type monoclinic ($C2/m$ space group) phase with 1% of Ni residing in the 4h lithium site or a composite structure consisting of 50% of Li_2MnO_3 type monoclinic ($C2/m$ space group) and 50% $LiMO_2$ (M = Co, Mn, Ni) type trigonal ($R\bar{3}m$ space group) structure. In the composite structure, 3% Li/Ni site exchange in the trigonal phase is also proposed. Further, temperature-dependent dc magnetic susceptibility shows Curie–Weiss paramagnetic behavior at $T \geq 100$ K, and no ordering/deviation of the field cooling (FC) curve in the temperature range 2–320 K indicates the random distribution of metal ions in the transition metal (TM) layer in the trigonal phase. Bifurcation of the zero-field cooling (ZFC) curve from the FC curve showing a magnetic ordering at $T_N \sim 50$ K reveals the presence of cation ordering in the TM layers arising from a distinct Li_2MnO_3-like phase. These results suggest that the lithium- and manganese-rich oxide with a composition $Li_{1.2}Mn_{0.55}Ni_{0.15}Co_{0.10}O_2$ is more likely a composite of monoclinic and trigonal phases. The report also highlights the unique materials diagnostic capability of combined ND and magnetic susceptibility techniques to obtain detailed structural information of complex oxide systems.

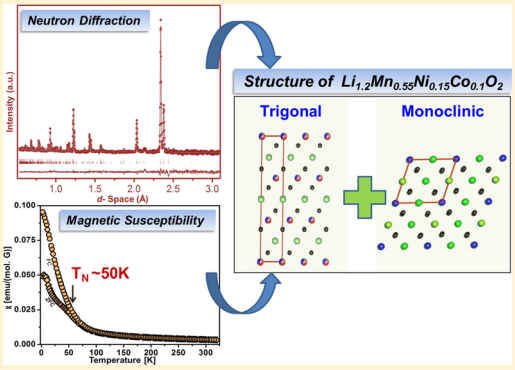

KEYWORDS: *lithium- and manganese-rich cathode, lithium ion batteries, neutron diffraction, magnetic ordering*

INTRODUCTION

In the realm of better performing and safer energy storage systems, lithium ion battery (LIB) technology has assumed to take the leading role for powering all-electric vehicles (EVs).[1] Compared to the stoichiometric lithium-based layered compounds (for example, $LiMn_{0.33}Ni_{0.33}Co_{0.33}O_2$), lithium- and manganese-rich nickel/manganese/cobalt (LMR-NMC) layered–layered cathode oxides have proved their ability to deliver higher voltage and higher energy density, which is theoretically more than 250 Ah kg^{-1} and 900 Wh kg^{-1} and remain the most promising candidates for LIBs in EV applications.[2]

The electrochemical performance of a high-voltage LIB is substantially affected by the crystal structure of the pristine cathode, especially when the cathode is a LMR-NMC type.[1b,2a,3] By applying (synchrotron) X-ray diffraction (XRD),[4] nuclear magnetic resonance (NMR),[5] and extended X-ray absorption fine structure (EXAFS) techniques,[6] researchers have proposed the structure of LMR-NMC as a composite of two phases: layered monoclinic Li_2MnO_3 ($C2/m$ space group) and layered trigonal or rhombohedral $LiMO_2$ ($R\bar{3}m$ space group) where M = Co, Mn, Ni. Recently, by advanced electron microscopy techniques[7] such as annular bright-field (ABF) scanning transmission electron microscopy (STEM) in combination with high-angle annular dark-field

Received: July 11, 2013
Revised: September 11, 2013
Published: September 12, 2013

   dx.doi.org/10.1021/cm402278q | *Chem. Mater.* 2013, 25, 4064–4070

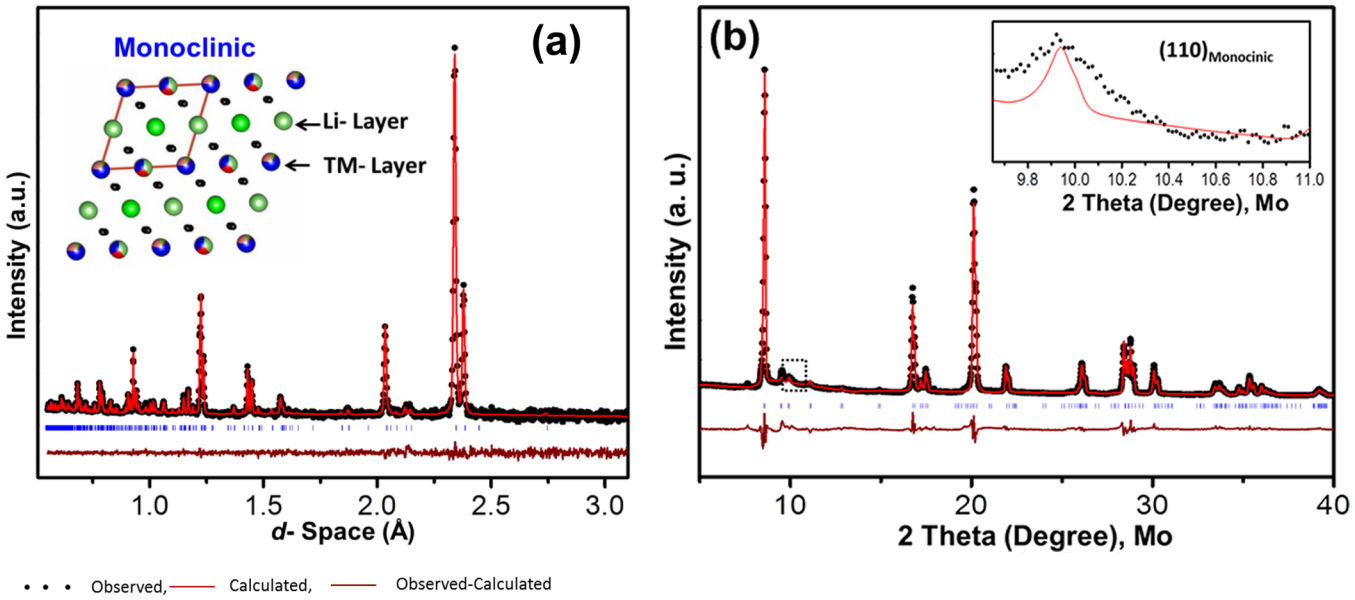

Figure 1. Refined powder neutron diffraction (a) and X-ray diffraction (b) for HE5050 by considering a monoclinic Li_2MO_3 (M = Co, Mn, Ni) unit cell. The different color of the atoms in the TM layer represents different TM ions (Co, Mn, Ni) present in same site. The inset in part b shows the anisotropic peak broadening along (110) planes in the monoclinic phase.

(HAADF) STEM, the intergrowth of both $LiMO_2$ and Li_2MnO_3-like phase and their heterosurface were revealed.[8] However, in another study using aberration-corrected STEM and diffraction-STEM, the structure of LMR-NMC was reported to be a solid solution between $LiMO_2$ and Li_2MnO_3 phase.[9] Although these advanced microscopy techniques have indubitably provided the structure of pristine LMR-NMC, the information is limited to the single particle domains, obscuring the complete crystallographic information of the bulk material. Additionally, X-ray diffraction methods are less sensitive to lower mass elements such as lithium and oxygen and are unable to provide the site occupancy factors of cation and anions. Therefore, the crystal structure of the LMR-NMC material remains enigmatic and is in a state of deliberation in the scientific community.

Unlike X-ray scattering, neutron interaction with materials is not atomic number (Z) dependent, so it is more sensitive to the lighter atoms in the presence of heavier atoms, thus making it possible to get more accurate structural information about lithium and oxygen in a TM ion environment. Direct current magnetic susceptibility plays an important role in determining the structure of oxide compounds by revealing different magnetic interaction (ordering) arising from various magnetically coupled metal ions (interlayer and intralayer interaction) that are present at specified sites in the unit cell. This work has employed the unique capabilities of combined neutron powder diffraction (ND) and magnetic susceptibility techniques for determining detailed crystallographic information of a LMR-NMC material having composition $Li_{1.2}Mn_{0.55}Ni_{0.15}Co_{0.01}O_2$ or TODA HE5050[2b,10] (HE5050 will be used hereafter). Recently, several issues such as voltage fade during subsequent cycles,[2b,10a,c,d,11] first cycle irreversible capacity,[2c,10a] and impedance rise during high-voltage hold[10b,12] with LMR-NMC have been identified and are believed to arise due to structure/phase transformation,[13] which hinders the practical application of these high-voltage cathodes. Therefore, there is a tremendous interest in the research community to understand these phenomena in order to suppress/mitigate these associated adverse effects.[2a] However, in order to understand structural transformation mechanisms during cycling, the detailed crystal structure of the pristine LMR-NMC must be understood, which remains perplexing and is the primary reason for this work. A few specific questions were addressed: (1) What is the structure of LMR-NMC oxide? (2) Is there any cation site interchange present in the unit cells? (3) How does the magnetic susceptibility play an important role for understanding the crystal structure of these complex oxide systems?

EXPERIMENTAL SECTION

The HE5050 powder was purchased from TODA America, Inc. The composition of the HE5050 was verified as $Li_{1.2}Mn_{0.55}Ni_{0.15}Co_{0.1}O_2$, and the ex situ XRD, particle morphology, selected area electron diffraction (SAED), high-resolution transmission electron microscopy image, and electrochemical performance data can be found in previous publications.[2b,10a,b,12] For neutron diffraction (ND), the HE5050 powder (~1 g) was placed in a 6 mm vanadium can in a glovebox containing helium. Room-temperature ND experiments were carried out on the POWGEN beamline at the Spallation Neutron Source[14] at Oak Ridge National Laboratory. The 24 sample changer was used to collect the room-temperature ND pattern using a frame of neutrons with center wavelength of 1.066 Å. The experimental pattern was refined by the Rietveld method using GSAS and the EXPGUI interface.[15] The ex situ powder XRD pattern was collected on a PANalytical X'Pert Pro system operated at 60 kV and 45 mA current with Mo Kα (0.710 73 Å) source, and a joint refinement with ND pattern was also performed by the Rietveld method using GSAS and the EXPGUI interface.[15] Direct current magnetization of the HE5050 powder was measured as a function of temperature, using a Quantum Design magnetic property measurement system. Each sample was first cooled to 2 K in zero field, then a field of 100 Oe was applied, and the data were collected from 2 to 320 K (zero-field-cooling mode, represented as ZFC). The sample was also cooled in the applied field from 320 K down to 2 K, while magnetization was measured (field-cooling mode, represented as FC).

dx.doi.org/10.1021/cm402278q | Chem. Mater. 2013, 25, 4064−4070

Table 1. Refined Crystallographic Parameters for TODA HE5050 with Monoclinic Li_2MO_3 (M = Co, Mn, Ni) Unit Cell

Composition: $Li_{1.199}Co_{0.099}Mn_{0.556}Ni_{0.140}O_2$[a]						
site	atom	x	y	z	SOF	U_{iso}
2c	Li	0	0	0.5	0.9957(11)	0.0117(2)
	Ni				0.0043(11)	
4h	Li	0	0.6551	0.5	0.9900(6)	0.0125(4)
	Ni				0.0100(6)	
2b	Li	0	0.5	0	0.364(8)	0.0029(2)
	Ni				0.2666(8)	
	Mn				0.3694(8)	
4g	Li	0	0.1660	0	0.128(12)	0.0076(4)
	Ni				0.0494(12)	
	Mn				0.6726(12)	
	Co				0.15(12)	
4i	O1	0.2226(8)	0	0.2232(8)	1	0.0049(4)
8j	O2	0.2539(5)	0.3223(9)	0.2256(5)	1	0.0056(8)

[a]Crystal system: monoclinic. Space group: $C2/m$. Lattice constants: a = 4.9456(19) Å, b = 8.5618(15) Å, c = 5.0314(13) Å. β = 109.2908(12)°, V = 201.086(5), Z = 12. Agreement parameters: R_{wp} = 5.05%, R_p = 8.69, χ^2 = 1.50.

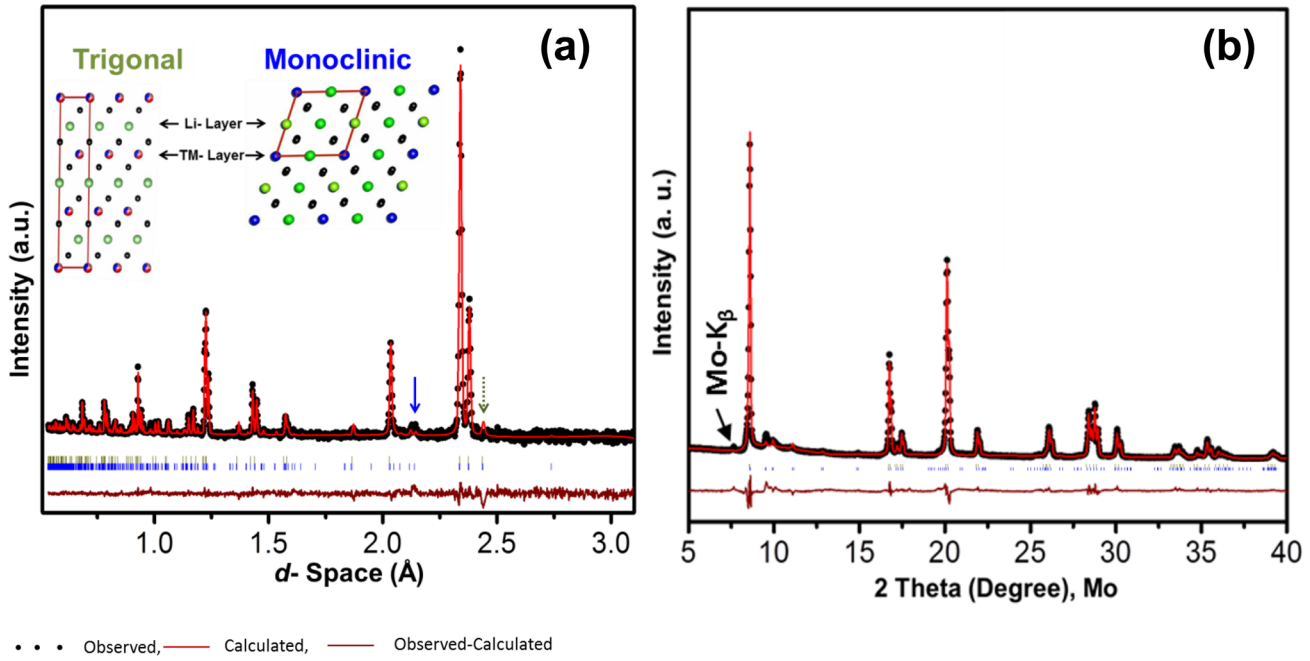

Figure 2. Refined powder neutron diffraction (a) and X-ray diffraction (b) for HE050 by considering a composite monoclinic Li_2MnO_3 and trigonal $LiMO_2$ (M = Co, Mn, Ni) unit cell. The different color of the atoms in the TM layer represents different TM ions (Co, Mn, Ni) present in same site. In part a, the solid arrow shows the cation-ordering peaks exclusively from the monoclinic Li_2MnO_3 unit cell and the dotted arrow represents the (101) reflection in the trigonal phase and (130)/(20$\bar{1}$) reflections in the monoclinic phase.

RESULTS AND DISCUSSION

Neutron Diffraction. Rietveld refinement of experimental ND patterns from the HE5050 powder was performed by using two models, viz., model 1, monoclinic ($C2/m$ space group), and model 2, monoclinic ($C2/m$) + trigonal ($R\bar{3}m$). The model with only the trigonal phase was not considered here since the experimental ND pattern contains ordering peaks (see the solid arrow in Figure 2) that could not be indexed by considering a trigonal phase alone.

Model 1: Monoclinic Phase with C2/m Space Group. In this model, the monoclinic phase with Li_2MnO_3 or Li-$[Li_{1/3}Mn_{2/3}]O_2$ composition ($C2/m$ space group) was used, and the refinement of experimental ND pattern was initiated by assuming one transition metal (Mn) atom present as explained by Strobel.[16] However, this resulted in poor agreement between data and the model (Figure S1, Supporting Information). The agreement parameters obtained were also unsatisfactory (R_{wp} = 13%, χ^2 = 11) since the HE5050 material contains Co and Ni along with Mn atoms, and the neutron scattering factors of these three metal atoms have much larger contrast (Mn, −3.73; Co, 2.49; and Ni, 10.3) compared to X-rays. Hence, assuming only Mn atom in Li_2MnO_3 type structure did not result in a reasonably good fit, as evidenced by Figure S1 (Supporting Information). Therefore, keeping the unit cell dimension unaltered, Mn, Co, and Ni were allowed to occupy the 2b and 4g sites (metal sites) and Li the 2c and 4h sites (lithium sites), which improved the profile fitting, as presented in Figure 1a. The positions of the oxygen were refined and the values showed no difference as compared to the values reported by Whitfield[17] and Strobel.[16] Interestingly, displacing only the Ni

dx.doi.org/10.1021/cm402278q | Chem. Mater. 2013, 25, 4064−4070

Table 2. Refined Crystallographic Parameters for TODA HE5050 with Combined Monoclinic Li_2MnO_3 and Trigonal $LiMO_2$ (M = Co, Ni, Mn) Unit Cells

site	atom	x	y	z	SOF	U_{iso}
Overall Composition: $Li_{1.20}Co_{0.1}Mn_{0.55}Ni_{0.15}O_2$[a]						
Phase 1 Composition: $LiCo_{0.25}Mn_{0.375}Ni_{0.375}O_2$. Crystal System: Trigonal. Space Group: $R\bar{3}m$. Phase Percentage: 50% (δ = 0.01)[b]						
3b	Li	0	0	0.5	1	0.0285(3)
3a	Co	0	0	0	0.25(4)	0.0345(3)
	Mn				0.375(4)	
	Ni				0.375(4)	
6c	O	0	0	0.2594 (20)	1	0.0093(6)
Phase 2 Composition: Li_2MnO_3. Crystal System: Monoclinic. Space Group: $C2/m$. Phase Percentage: 50% (δ = 0.01)[c]						
2c	Li	0	0	0.5	1	0.0132(2)
4h	Li	0	0.6606	0.5	1	0.0132(2)
2b	Li	0	0.5	0	1	0.0132(4)
4g	Mn	0	0.1670	0	1	0.0101(4)
4i	O	0.2189(10)	0	0.2283(9)	1	0.0027(4)
8j	O	0.2548(7)	0.3202(20)	0.2243(6)	1	0.0048(8)

[a]Agreement parameters: R_{wp} = 5.05%, R_p= 8.09, χ^2 = 1.50. [b]Lattice constants: $a = b$ = 2.85525(12) Å, c = 14.2483(10) Å. V = 100.596(7), Z = 3. [c]Lattice constants: a = 4.9464(27) Å, b = 8.5624(5) Å, c = 5.0332(21) Å. β = 109.3221(32)°, V = 201.186(9), Z = 4.

(not Co and Mn) from TM sites to the lithium sites showed significant improvement in the fits, and good agreement parameters were achieved. Site occupancy factors (SOF) of all individual atoms were refined by applying atomic position and displacement parameter constraints to the particular sites. The crystallographic information obtained from these refinements is presented in Table 1. It was observed that the 2b sites are rich in Ni as compared to the 4g sites. It is believed that Ni atoms prefer the lithium sites, and this preference might be due to similar ionic radii of Ni^{2+} and Li^+ in an octahedral coordination. On the basis of model 1, the structural parameter of HE5050 can be represented as $\{Li_{1-x}Ni_x\}^{2c}\{Li_{1-y}Ni_y\}^{4h}[\{Li_{0.364}Ni_{0.266}Mn_{0.3694}\}^{2b}\{Li_{0.128}Ni_{0.0494}Mn_{0.6726}Co_{0.15}\}^{4g}]O^{4i}O^{8j}$, where x = 0.0043 and y = 0.01. The overall composition was calculated as $Li_{1.199}Co_{0.099}Mn_{0.556}Ni_{0.140}O_2$, which is in good agreement with its composition from energy dispersive X-ray analysis reported elsewhere.[12]

In this model, both Li and Mn site occupancies were refined and the neutron scattering lengths between these two atoms differ by a small amount (Li, −1.9; Mn, −3.73); therefore, in order to validate these occupancies, a XRD pattern of HE5050 material was refined simultaneously with the ND pattern without altering the crystallographic information. The refined XRD pattern is presented in Figure 1b (the refined ND diffraction remained similar to Figure 1a) and shows a very good match between the experimental and calculated pattern. However, the refined XRD pattern revealed the anisotropically peak broadening[18] and a prominent observation was made along (200) and (110) monoclinic phase reflections (for example, the (110) monoclinic peak is shown as an inset in Figure 1b), which are consistent with the presence of stacking faults in the transition metal layers and/or at the domain boundaries of two phases (see the model 2 discussion below). The evidence of stacking fault in layered−layered LMR HE5050 compound is consistent with observations in similar layered compounds as identified in previous reports.[8,17,19]

Model 2: Monoclinic Phase with C2/m Space Group and Trigonal Phase with R$\bar{3}$m Space Group. Model 2 is a composite structure comprising a trigonal phase (space group $R\bar{3}m$) with $LiMO_2$ (M = Mn, Co, Ni) composition and a monoclinic phase (space group $C2/m$) with Li_2MnO_3 composition as shown in Figure 2. Placing three transition metal atoms in the metal sites in the monoclinic phase resulted in a negligible phase fraction (1%) for the trigonal phase, in which case it is effectively the same as model 1 (monoclinic phase only). Hence, in model 2, unlike in model 1, only Mn was allowed in the 4g site of the monoclinic phase, while all the transition metal atoms were allowed in 3a sites in the trigonal phase, similar to the composite notation $xLiMO_2\cdot(1-x)$-Li_2MnO_3, where M = Co, Mn, Ni. The lattice parameters and oxygen atom positions with temperature factors (U_{iso}) were refined, and the values are reported in the Table 2. In the trigonal phase, the lithium occupancy in the 3b site was fixed at 1 and the occupancies of Co, Mn, Ni in the 3a site were refined with a constraint that the site was fully occupied. In the monoclinic phase, a lithium atom was assumed to be present in the lithium site (2c and 4h) and metal site (2b), and Mn was allowed to reside in the 4g metal site (model based on Strobel[16]). The obtained crystallographic parameters are presented in Table 2. It was observed that the small peaks in the experimental pattern with a d spacing of 2.12 and 2.14 Å could only be refined with monoclinic phase and correspond to (040) and (22$\bar{1}$) lattice planes, respectively. These reflections indicate the cation-ordering of Li with the Mn ions in the transition metal layer to form a Li_2MnO_3-like component in HE5050 compound. The refined composition based on model 2 was calculated as $0.50LiCo_{0.25}Mn_{0.375}Ni_{0.375}O_2\cdot0.50Li_2MnO_3$ which gives an overall composition of $Li_{1.20}Co_{0.1}Mn_{0.55}Ni_{0.15}O_2$. This is also in agreement with the composition obtained in model 1 and the previous results from EDS.[12]

Interestingly, in model 2, one extra reflection corresponding to a d-spacing of 2.44 Å (see the dotted arrow in Figure 2a) was observed in the calculated pattern; however, it was not observed in the experimental pattern. This peak was assigned to a (101) reflection in the trigonal phase and (130)/(20$\bar{1}$) reflections in the monoclinic phase. To address this intriguing observation, model 2a was proposed, which is similar to the model 2. In model 2a, however, the Li/Mn atoms in the monoclinic phase and Li/Ni atoms in the trigonal phase were allowed to exchange sites between lithium and transition metal layers. Allowing Li/Mn to exchange in the monoclinic phase did not alter the peak intensity of this extra reflection, but when Li and Ni atoms were exchanged between Li/Ni sites in the

dx.doi.org/10.1021/cm402278q | Chem. Mater. 2013, 25, 4064−4070

trigonal phase, the intensity of this reflection was minimized in the calculated pattern (see parts a and b of Figure 3 for comparison). At this stage, only the occupancy of Li and Ni was varied while Mn and Co occupancies were kept constant, and refinement showed that 3% of the Li site could be occupied by Ni. Further increasing this value did not result in significant improvement in the fit. The refined crystallographic parameter in trigonal system after considering the Li/Ni interchange is presented in Table 3. The Li/Ni exchange in the HE5050 material is consistent with the selected area electron diffraction data[12] reported previously. In this case, the total composition remained unaltered. Hence in a two-component system, the pristine HE5050 LMR-NMC compound can be written as $0.50\{Li_{1-x}Ni_x\}\{Li_xCo_{0.25}Mn_{0.375}Ni_{0.375-x}\}O_2{\cdot}0.50Li_2MnO_3$, where $x = 0.0354$. Similar to the model 1, with keeping this model unaltered, the simultaneous refinement of XRD and ND patterns of HE5050 were performed, and the refined XRD pattern (the refined ND diffraction remained similar to Figure 2a) is presented in the Figure 2b, which shows a very good agreement with the model. The anisotropic peak broadening was also observed in the refined XRD pattern similar to the observation made in model 1 (see Figure S2, Supporting Information) and indicates the presence of a stacking fault in the HE5050 compound. These stacking faults may change the symmetry, which may induce the pathway to form trigonal and monoclinic unit cells with local domains in a single particle.

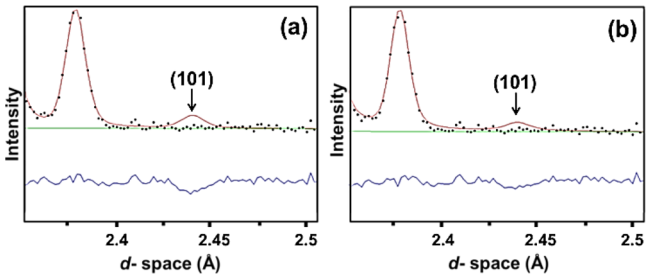

Figure 3. Trigonal (101) plane intensity before Li/Ni exchange (a) and after 3% Li/Ni exchange (b).

Table 3. Refined Crystallographic Information from Trigonal Phase after 3% Li/Ni Exchange[a,b]

site	atom	x	y	z	SOF	U_{iso}
3b	Li	0	0	0.5	0.9646(5)	0.0285(4)
	Ni				0.0354(5)	
3a	Co	0	0	0	0.25	0.03453(8)
	Mn				0.375	
	Ni				0.3396	
	Li				0.0354	
6c	O	0	0	0.25941(8)	1	0.00931(4)

[a]The monoclinic phase information was similar to the results reported in Table 2. [b]Agreement parameters: R_{wp} = 5.05%, R_p= 6.69, χ^2 = 1.50. Crystal system: trigonal. Space group: $R\bar{3}m$. Lattice constants: $a = b$ = 2.85525(12) Å, c = 14.2483(10) Å. V = 100.596(7), Z = 3.

Magnetic Susceptibility. Both of the models (model 1 with the monoclinic phase only and model 2 with a mixture of the monoclinic and trigonal phases) fit the neutron diffraction data equally well. Therefore, temperature-dependent magnetic susceptibility measurements were performed to determine which model is more accurate. Temperature-dependent dc magnetic susceptibility from HE5050 powder collected in FC and ZFC mode is given in figure 4. From the plot, it is obvious that the compound shows a Curie–Weiss paramagnetic behavior at higher temperature, $T \geq 100$ K (see the inset in Figure 4 for Curie–Weiss fit between T = 100 and 320K) and at this temperature range, the FC and ZFC curves follows the same path, indicating the random distribution of TM ions in the TM layer. In fact, this suggests that there are certain regimes where cation-ordering in the TM layer is absent, which leads to the presence of trigonal $LiMO_2$ phase (M = Co, Mn, Ni). At lower temperature ($T \leq 100$ K), the magnetic susceptibility value increases, and eventually a bifurcation of FC and ZFC curves occurs at transition temperature (T_N) ~50 K, confirming a magnetic ordering in the structure, which is more likely originated from the Li_2MnO_3 phase.[16,20] Such a magnetic ordering is not possible in the case of only layered trigonal phase (e.g., $LiMn_{0.33}Ni_{0.33}Co_{0.33}O_2$), since in the trigonal phase, Co, Mn, and Ni ions are randomly distributed in the TM layer[21] and FC and ZFC curves follows the same path in the experimental temperature range T = 2–300 K. The magnetic ordering in HE5050 confirms the presence of clusters of an additional phase that is thought to be a Li_2MnO_3-like compound. The θ_c calculated for HE5050 material is −41 K which is an indication of the antiferromagnetic nature in the material. In an Li_2MnO_3 phase, octahedral $Mn^{4+}(d_3)$ share edges and a 90° $Mn^{4+}(d_3)$–O–$Mn^{4+}(d_3)$ interaction (see S3, Supporting Information) is possible, which is strongly antiferromagnetic (AFM) based on Goodenough's rule.[22]

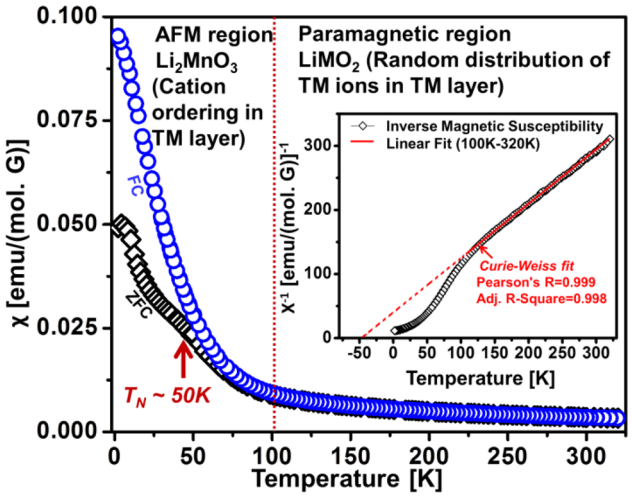

Figure 4. Temperature-dependent molar magnetic susceptibility of HE5050 at H = 100 Oe. The inset shows the Curie–Weiss fit to the inverse magnetic susceptibility data in T = 100–320 K range showing the paramagnetic region. The bifurcation of FC and ZFC at T_N = 50 K confirms the magnetic ordering due to the presence of monoclinic Li_2MnO_3 type lattice.

The behavior of the magnetic susceptibility curve below the transition temperature might be an indication of spin glass behavior with a magnetic frustrated lattice.[21b] However, for a spin glass system with a magnetic frustrated lattice, the value of $|\theta_c|/T_f > 10$ (where θ_c is the Curie–Weiss temperature and T_f = freezing temperature) as explained elsewhere.[23] In the case of HE5050 material (in this work), $|\theta_c|/T_N < 1$, which indicates that spin glass and/magnetic frustration might be impossible in the lattice. Moreover, in case of pure Li_2MnO_3 (monoclinic phase), where cation-ordering is present in the TM layer, the

dx.doi.org/10.1021/cm402278q | Chem. Mater. 2013, 25, 4064–4070

antiferromagnetic transition was observed in both the FC and ZFC curves, where both the curves follow the same path below the transition temperature.[24] In the case of pure trigonal phase, where cation ordering is not present in the transition metal layer (for example, $LiMn_{1/3}Ni_{1/3}Co_{1/3}O_2$), no magnetic ordering is observed at low temperature and FC and ZFC follow the same path over the temperature range.[21] In composite HE5050 (material in this study), magnetic ordering is observed and a magnetic transition occurs at $T_N \sim 50$ K; however, the FC curve follows the path as observed for $LiMn_{1/3}Ni_{1/3}Co_{1/3}O_2$, whereas ZFC follows the path like Li_2MnO_3, supporting our hypothesis that the HE5050 compound is a mixture of these two phases. The presence of trigonal and monoclinic phase in HE5050 material is also consistent with the selected area electron diffraction (SAED) pattern as reported previously.[10a] In that SAED pattern, the particle oriented along the [0001] zone axis showed a set of fundamental reflections originating from the trigonal phase, and weak "triplet" reflections appeared half way between two fundamental reflections, which suggested the presence of the monoclinic phase.[10a] On the basis of the above facts, it is now confirmed that the HE5050 LMR-NMC is more like likely a composite between trigonal and monoclinic phases.

CONCLUSIONS

Despite great success in synthesizing LMR-NMC compounds, the parent crystal structure remained elusive. Neutron diffraction and magnetic susceptibility in this study were employed to deduce detailed crystallographic information of a LMR-NMC type compound having formula of $Li_{1.2}Mn_{0.55}Ni_{0.15}Co_{0.10}O_2$. The conclusions from this work are given as follows:

(I) The experimental neutron diffraction data reveal good fits with only monoclinic system with Li_2MO_3 (M = Co, Mn, Ni) or composite phase between trigonal $LiMO_2$ (M = Co, Mn, Ni) and monoclinic Li_2MnO_3 structure.

(II) The composition of LMR-NMC HE5050 was found to be $\{Li_{1-x}Ni_x\}^{2c}\{Li_{1-y}Ni_y\}^{4h}[\{Li_{0.364}Ni_{0.266}Mn_{0.3694}\}^{2b}\{Li_{0.128}Ni_{0.0494}Mn_{0.6726}Co_{0.15}\}^{4g}]O^{4i}O^{8j}$, where $x = 0.0043$ and $y = 0.01$, in one-component Li_2MO_3 (M = Co, Mn, Ni) compound and $0.50\{Li_{1-x}Ni_x\}\{Li_xCo_{0.25}Mn_{0.375}Ni_{0.375-x}\}O_2 \cdot 0.50Li_2MnO_3$, where $x = 0.0354$, in a composite structure.

(III) Li/Ni exchange between Li and metal layer was observed irrespective to the single phase or composite phase models. One percent of Ni residing in the lithium site in Li_2MO_3 model (model 1 in ND simulation) and 3% Li/Ni site exchange in the trigonal structure of composite model (model 2 in ND simulation) were calculated.

(IV) Temperature-dependent magnetic susceptibility revealed the Curie–Weiss paramagnetic nature at higher temperature, suggesting the trigonal $LiMO_2$ phase, and magnetic ordering was observed at lower temperature with a magnetic transition at $T_N \sim 50$ K, which is attributed to solely Li_2MnO_3-like phase and manifest that the structure is more likely a composite between two phases (model 2 in ND simulation).

To summarize the relation between the questions asked in the Introduction and the conclusions drawn, conclusions I, II, and IV answer question 1; conclusions II and III answer the question 2; and conclusion IV answers the question 3.

This work demonstrates the effectiveness of complementary techniques to understand highly complex cathode oxide structures and sheds light on the phases present in LMR-NMC cathode materials. The crystallographic information provided here may be helpful for determining the structure of cycled LMR-NMC to understand the voltage fade problem and first cycle irreversible capacity.

ASSOCIATED CONTENT

Supporting Information

Refined neutron diffraction pattern and unit cell of Li_2MnO_3 showing the Mn–O–Mn interaction. This material is available free of charge via the Internet at http://pubs.acs.org.

AUTHOR INFORMATION

Corresponding Authors

*E-mail: mohantyd@ornl.gov (D.M.).
*E-mail: danielc@ornl.gov (C.D.).

Notes

The authors declare no competing financial interest.

ACKNOWLEDGMENTS

This research at Oak Ridge National Laboratory, managed by UT Battelle, LLC, for the U.S. Department of Energy (DOE) under contract DE-AC05-00OR22725, was sponsored by the Vehicle Technologies Office Applied Battery Research Program (Program Managers Peter Faguy and David Howell) of the Office of Energy Efficiency and Renewable Energy. This research was supported by the DOE Office of Basic Energy Sciences, Materials Sciences and Engineering Division and by ORNL's User Facility at the Spallation Neutron Source, which is sponsored by the Scientific User Facilities Division, Office of Basic Energy Sciences. The TODA HE5050 material was obtained from Argonne National Laboratory in collaboration with Andrew Jansen and Bryant Polzin. The authors thank Dr. Jason R. Croy from Argonne National Laboratory for his valuable suggestions on structural analysis.

REFERENCES

(1) (a) Goodenough, J. B. *J. Am. Chem. Soc.* **2013**, *135*, 1167. (b) Whittingham, M. S. *Mater. Res. Bull.* **2008**, *33*, 411. (c) Daniel, C. *JOM* **2008**, *60*, 43. (d) Tarascon, J. M.; Armand, M. *Nature* **2008**, *451*, 652.

(2) (a) Yu, H.; Zhou, H. *J. Phys. Chem. Lett.* **2013**, *4* (1268), 1268. (b) Li, Y.; Bettge, M.; Polzin, B.; Zhu, Y.; Balasubramanian, M.; Abraham, D. P. *J. Electrochem. Soc.* **2013**, *160* (5), A3006. (c) Yabuuchi, N.; Yoshii, K.; Myung, S.-T.; Nakai, I.; Komaba, S. *J. Am. Chem. Soc.* **2011**, *133*, 4404.

(3) (a) Johnson, C. S.; Li, N.; Lefief, C.; Vaughey, J. T.; Thackeray, M. M. *Chem. Mater.* **2008**, *20*, 6095. (b) Thackeray, M. M.; Kang, S.-H.; Johnson, C. S.; Vaughey, J. T.; Benedek, R.; Hackney, S. A. *J. Mater. Chem.* **2007**, *17*, 3112.

(4) Yu, H. J.; Kim, H. J.; Wang, Y. R.; He, P.; Asakura, D.; Nakamura, Y.; Zhou, H. S. *Phys. Chem. Chem. Phys.* **2012**, *14*, 6584.

(5) Pan, C. J.; Lee, Y. J.; Ammundsen, B.; Grey, C. P. *Chem. Mater.* **2002**, *14*, 2289.

(6) Bareno, J.; Lei, C. H.; Wen, J. G.; Kang, S. H.; Petrov, I.; Abraham, D. P. *Adv. Mater.* **2010**, *22*, 1122.

(7) Bareno, J.; Balasubramanian, M.; Kang, S. H.; Wen, J. G.; Lei, C. H.; Pol, S. V.; Petrov, I.; Abraham, D. P. *Chem. Mater.* **2011**, *23*, 2039.

(8) Yu, H.; Shikawa, R.; So, Y-G; Shibata, N.; Kudo, T.; Zhou, H.; Ikuhara, Y. *Angew. Chem.* **2013**, *52*, 5969.

(9) Jarvis, K. A.; Deng, Z.; Allard, L. F.; Manthiram, A.; Ferreira, P. J. *Chem. Mater.* **2011**, *23*, 3614.

(10) (a) Mohanty, D.; Kalnaus, S.; Meisner, R. A.; Rhodes, K. J.; Li, J.; Payzant, E. A.; Wood, D. L., III; Daniel, C. *J. Power Sources* **2013**, *229*, 239–248. (b) Mohanty, D.; Kalnaus, S.; Meisner, R. A.; Sefat, A. S.; Li, J.; Payzant, E. A.; Rhodes, K.; Wood, D., III; Daniel, C. *RSC Adv.*

2013, *3*, 7479. (c) Croy, J. R.; Gallagher, K. G.; Balasubramanian, M.; Chen, Z.; Ren, Y.; Kim, D.; Kang, S. H.; Dees, D. W.; Thackeraya, M. M. *J. Phys. Chem. C* **2013**, *117* (13), 6525. (d) Gallaghera, K. G.; Croy, J. R.; Balasubramanian, M.; Bettge, M.; Abraham, D. P.; Burrell, A. K.; Thackeray, M. M. *Electrochem. Commun.* **2013**, *33*, 96.

(11) Martha, S. K.; Nanda, J.; Veith, G. M.; Dudney, N. J. *J. Power Sources* **2012**, *199*, 220.

(12) Mohanty, D.; Sefat, A. S.; Kalnaus, S.; Li, J.; Meisner, R. A.; Abraham, D. P.; Payzant, E. A.; Wood, D. L., III; Daniel, C. *J. Mater. Chem. A* **2013**, *1*, 6249.

(13) Boulineau, A.; Simonin, L.; Colin, J. F.; Canevet, E.; Daniel, L.; Patoux, S. *Chem. Mater.* **2012**, *24*, 3558.

(14) Huq, A.; Hodges, J. P.; Gourdon, O.; Heroux, L. *Z. Kristallogr. Proc.* **2011**, *1*, 127.

(15) (a) Toby, B. H. *J. Appl. Crystallogr.* **2001**, *34*, 210. (b) Larsen, A. C.; Von Dreele, R. B. General Structure Analysis System (GSAS). *Los Alamos National Laboratory Report LAUR 86-748;* 2004.

(16) Strobel, P.; Andron, B. L. *J. Solid State Chem.* **1988**, *75*, 90.

(17) Whitfield, P. S.; Davidson, I. J.; Stephens, P. W.; Cranswick, L. M .D.; Swainson, I. P. *Z. Kristallogr. Suppl.* **2007**, *26*, 483.

(18) Stephens, P. W. *J. Appl. Crystallogr.* **1999**, *32*, 281−289.

(19) Bréger, J.; Jiang, M.; Dupré, N.; Meng, Y. S.; Shao-Horn, Y.; Ceder, G.; Grey, C. P. *J. Solid State Chem.* **2005**, *178*, 2575−2585.

(20) Lee, S.; Choi, S.; Kim, J.; Sim, H.; Won, C.; Lee, S.; Hur, N.; Park, J.-G. *J. Phys. Condens. Matter* **2012**, *24*, 456004.

(21) (a) Mohanty, D.; Gabrisch, H. *J. Power Sources* **2012**, *220*, 405. (b) Chernova, N. A.; Ma, M.; Xiao, J.; Whittingham, M. S.; Breger, J.; Grey, C. P. *Chem. Mater.* **2007**, *19*, 4682.

(22) Goodenough, J. B. *Phys. Rev.* **1960**, *117*, 1442.

(23) Greedan, J. E. *J. Mater. Chem.* **2001**, *11*, 37.

(24) Sugiyama, J.; Mukai, K.; Nozaki, H.; Harada, M.; Månsson, M.; Kamazawa, K.; Andreica, D.; Amato, A.; Hillier, A. D. *Phys. Rev. B* **2013**, *87*, 024409.